Electronic Supplementary Information for:

Spectroscopic Properties and Reactivity of a Mononuclear Oxomanganese(IV) Complex

*Domenick F. Leto, Rena Ingram, Victor W. Day, and Timothy A. Jackson**

Department of Chemistry, University of Kansas, 1251 Wescoe Hall Drive, Lawrence, KS 66045

1. Materials.

All chemicals and solvents were obtained from commercial vendors and were ACS reagent-grade or better and used as received, except for 9,10-dihydroanthracene (DHA) which was recrystallized from ethanol.[1] All solvents were dried and degassed according to published procedures.[1] $H_2{}^{18}O$ (97% ^{18}O-enriched) was purchased from ICON Services Inc. (Summit, NJ, USA). d_4-DHA was synthesized as previously reported.[2]

2. Synthesis and characterization of $[Mn^{II}(N4py)(OTf)](OTf)$ and $[Mn^{IV}(O)(N4py)]^{2+}$.

Preparation of Complexes. The synthesis of the N4py ligand was performed according to a previously described procedure.[3-4] The triflate salt of **1**, $[Mn^{II}(N4py)(OTf)](OTf)$, was synthesized by reacting the N4py ligand (N4py = *N*,*N*-bis(2-pyridylmethyl)-*N*-bis(2-pyridyl)methylamine) with $Mn^{II}(OTf)_2$ in an acetonitrile (CH_3CN) solution in a 1:1 molar ratio overnight in a dry-box as previously reported.[5] The resulting solution was filtered and purified by recrystallization with diethyl ether. Single crystals suitable for X-ray analysis were obtained by slow diffusion of diethyl ether to a solution of **1** in acetonitrile (overall yield 90%). Elemental analysis for $[Mn^{II}(N4py)(OTf)](OTf)\bullet 0.5CH_3CH_2OH$: $MnC_{26}H_{24}N_5O_{6.5}F_6S_2$ calc. (%): C 42.00, H 3.25, N 9.42; found (%): C 42.16, H 3.61, N 9.68. Elemental analysis was performed by Columbia Analytical Services, Tuscon, Arizona.

The $[Mn^{IV}(O)(N4py)]^{2+}$ complex (**2**) was prepared by adding 2.5 equivalents (2.2 mg, 0.01 mmol) of iodosylbenzene (PhIO) to a 2 mM (2.9 mg, 0.004 mmol) solution of $\mathbf{1}(OTf)_2$ in 2,2,2-trifluoroethanol (CF_3CH_2OH) at 25 ^oC under an Ar atmosphere. The formation of the new green species **2** was complete in 10 minutes with the formation of a broad electronic absorption band at 950 nm and weak shoulders at 600 and 450 nm. Complex **2** was less stable under an Ar atmosphere ($t_{1/2} \approx 0.5$ h at 25 ^oC) than in air ($t_{1/2} \approx 2.75$ h at 20 ^oC). Electronic absorption spectra were obtained on either a Varian Cary 50 Bio or an Agilent 8453 spectrophotometer, both of which were interfaced with a Unisoku cryostat (USP-203-A) capable of maintaining temperatures between 150 and 373 K.

X-ray Crystallography of [Mn^{II}(N4py)(OTf)](OTf). Yellow crystals of $[Mn(C_{23}H_{21}N_5)(O_3SCF_3)]_2[O_3SCF_3][ClO_4]$ are, at 100(2) K, monoclinic, space group $P2_1 - C_2^2$ (No. 4)[6] with **a** = 10.178(3) Å, **b** = 19.832(5) Å, **c** = 14.229(4) Å, **β** = 107.156(4)°, V = 2744(1) $Å^3$ and Z = 2 formula units {d_{calcd} = 1.684 g/cm^3; μ_a(MoKα) = 0.728 mm^{-1}}. A full hemisphere of diffracted intensities (1850 10-second frames with an ω scan width of 0.30°) was measured for a single-domain specimen using graphite-monochromated MoKα radiation (λ= 0.71073 Å) on a Bruker SMART APEX CCD Single Crystal Diffraction System.[7] X-rays were provided by a fine-focus sealed x-ray tube operated at 50 kV and 30 mA. Lattice constants were determined with the Bruker SAINT software package using peak centers for 7778 reflections. A total of 25171 integrated reflection intensities having 2θ((MoKα)< 58.36° were produced using the Bruker program SAINT;[8] 13119 of these were unique and gave R_{int} = 0.058 with a coverage which was 92.7% complete. The data were corrected empirically for variable absorption effects using equivalent reflections; the relative transmission factors ranged from 0.926 to 1.000. The Bruker software package SHELXTL was used to solve the structure using "direct methods" techniques. All stages of weighted full-matrix least-squares refinement were conducted using F_o^2 data with the SHELXTL Version 6.10 software package.[9]

The final structural model incorporated anisotropic thermal parameters for all nonhydrogen atoms and isotropic thermal parameters for all hydrogen atoms. All hydrogen atoms were included in the structural model as idealized atoms (assuming sp^2- or sp^3-hybridization of the carbon atoms and C-H bond lengths of 0.95 - 1.00 Å). The isotropic thermal parameters of all hydrogen atoms were fixed at values 1.2 times the equivalent isotropic thermal parameter of the carbon atom to which they are covalently bonded. A total of 784 parameters were refined using 1 restraint, 13119 data and weights of $w = 1/ [\sigma^2(F^2) + (0.0580\ P)^2]$ where $P = [F_O^2 + 2F_C^2] / 3$. Final agreement factors at convergence are: R_1(unweighted, based on F) = 0.060 for 10673 independent absorption-corrected "observed" reflections having 2θ(MoKα) < 58.36° and I > 2σ(I); R_1(unweighted, based on F) = 0.074 and wR_2(weighted, based on F^2) = 0.125 for all 13119 independent absorption-corrected reflections having 2θ(MoKα) < 58.36°. The largest shift/s.u. was 0.000 in the final refinement cycle. The final difference map had maxima and minima of 0.88 and -0.44 $e^-/Å^3$, respectively. The absolute structure was determined experimentally using anomalous dispersion of the x-rays; the Flack absolute structure parameter refined to a final value of 0.00(2).

The asymmetric unit contains two $[Mn(C_{23}H_{21}N_5)(O_3SCF_3)]^+$ cations, one $(O_3SCF_3)^-$ anion and one $(ClO_4)^-$ anion. The $(ClO_4)^-$ anion was introduced in one of the final steps in the ligand synthesis when the N4py perchlorate salt is isolated.[3-4] CCDC-885972 contains the supplementary crystallographic data for [Mn(N4py)(OTf)](OTf). This data can be obtained free of charge from the Cambridge Crystallographic Data Centre via www.cccdc.cam.ac/data_request/cif.

Table S1. Crystal data and structure refinement for $[Mn(C_{23}H_{21}N_5)(O_3SCF_3)]_2[O_3SCF_3][ClO_4]$.

Empirical formula	$C_{49}H_{42}ClF_9Mn_2N_{10}O_{13}S_3$	
Formula weight	1391.44	
Temperature	100(2) K	
Wavelength	0.71073 Å	
Crystal system	Monoclinic	
Space group	$P2_1 - C_2^2$ (No. 4)	
Unit cell dimensions	**a** = 10.178(3) Å	**α** = 90000°
	b = 19.832(5) Å	**β** = 107.156(4)°
	c = 14.229(4) Å	**γ** = 90.000°
Volume	2744.4(12) $Å^3$	
Z	2	
Density (calculated)	1.684 Mg/m^3	
Absorption coefficient	0.728 mm^{-1}	
F(000)	1412	
Crystal size	0.26 x 0.26 x 0.13 mm^3	
Theta range for data collection	2.42° to 29.18°	
Index ranges	$-13 \le h \le 13$, $-27 \le k \le 27$, $-19 \le l \le 18$	
Reflections collected	25171	
Independent reflections	13119 [R_{int} = 0.058]	
Completeness to theta = 29.18°	92.7 %	
Absorption correction	Multi-scans	
Max. and min. transmission	1.000 and 0.926	
Refinement method	Full-matrix least-squares on F^2	
Data / restraints / parameters	13119 / 1 / 784	
Goodness-of-fit on F^2	0.988	
Final R indices [I>2sigma(I)]	R_1 = 0.060, wR_2 = 0.119	
R indices (all data)	R_1 = 0.074, wR_2 = 0.125	
Absolute structure parameter	0.000(15)	
Largest diff. peak and hole	0.88 and -0.44 $e^-/Å^3$	

$R_1 = \Sigma \, ||F_o| - |F_c|| \, / \, \Sigma \, |F_o|$

$wR_2 = \{ \, \Sigma \, [w(F_o^2 - F_c^2)^2] \, / \, \Sigma \, [w(F_o^2)^2] \, \}^{1/2}$

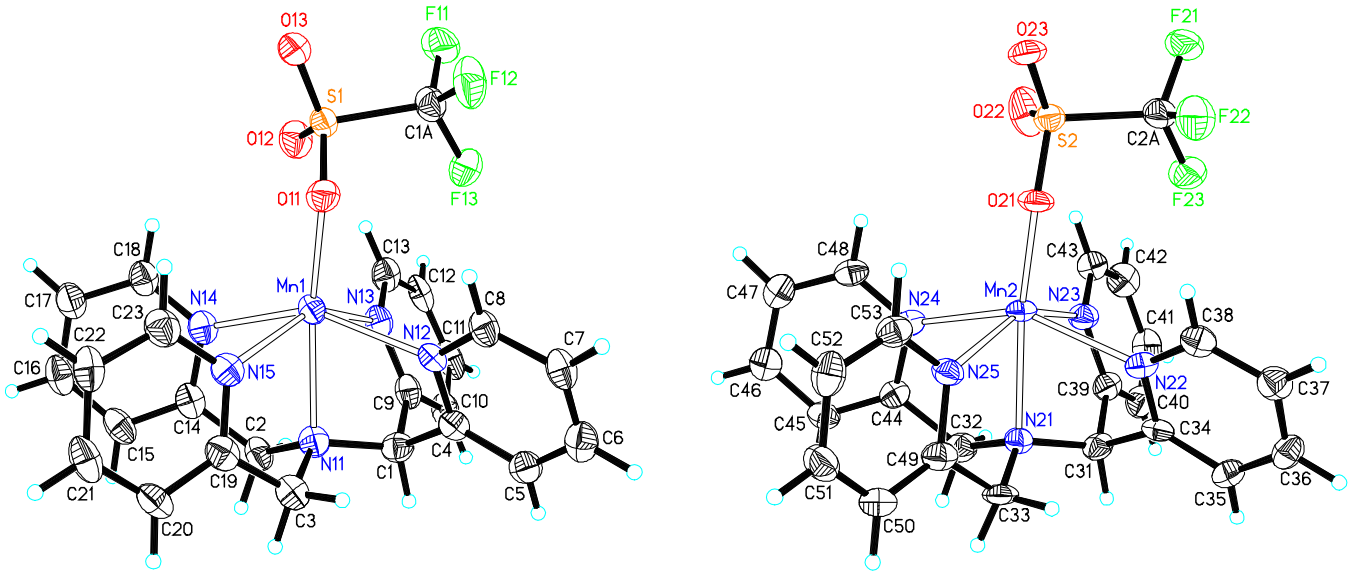

Figure S1. Molecular structures of the two $[Mn^{II}(N4py)(OTf)]^{+}$ cations found in the asymmetric unit of $[Mn(C_{23}H_{21}N_5)(O_3SCF_3)]_2[O_3SCF_3][ClO_4]$, showing 50% probability ellipsoids.

Table S2. Selected bond lengths (Å) and angles (°) for $[Mn(C_{23}H_{21}N_5)(O_3SCF_3)]_2[O_3SCF_3][ClO_4]$.

Mn(1)-O(11)	2.125(3)	O(11)-Mn(1)-N(14)	116.80(13)	N(14)-Mn(1)-N(11)	76.53(14)
Mn(1)-N(14)	2.255(4)	O(11)-Mn(1)-N(13)	117.19(13)	N(13)-Mn(1)-N(15)	148.25(14)
Mn(1)-N(13)	2.271(4)	O(11)-Mn(1)-N(15)	94.42(12)	N(13)-Mn(1)-N(12)	81.18(13)
Mn(1)-N(15)	2.271(4)	O(11)-Mn(1)-N(12)	92.09(12)	N(13)-Mn(1)-N(11)	74.17(13)
Mn(1)-N(12)	2.278(4)	O(11)-Mn(1)-N(11)	161.24(13)	N(15)-Mn(1)-N(12)	95.63(13)
Mn(1)-N(11)	2.289(4)	N(14)-Mn(1)-N(13)	88.81(13)	N(15)-Mn(1)-N(11)	74.57(13)
		N(14)-Mn(1)-N(15)	76.68(13)	N(12)-Mn(1)-N(11)	74.32(13)
		N(14)-Mn(1)-N(12)	150.76(14)	S(1)-O(11)-Mn(1)	119.9(2)
Mn(2)-O(21)	2.107(3)	O(21)-Mn(2)-N(24)	115.8(1)	N(24)-Mn(2)-N(21)	76.1(1)
Mn(2)-N(24)	2.247(4)	O(21)-Mn(2)-N(23)	116.0(1)	N(23)-Mn(2)-N(25)	150.5(1)
Mn(2)-N(23)	2.265(4)	O(21)-Mn(2)-N(25)	93.1(1)	N(23)-Mn(2)-N(22)	79.9(1)
Mn(2)-N(25)	2.231(4)	O(21)-Mn(2)-N(22)	94.4(1)	N(23)-Mn(2)-N(21)	74.7(1)
Mn(2)-N(22)	2.288(4)	O(21)-Mn(2)-N(21)	162.8(1)	N(25)-Mn(2)-N(22)	93.5(1)
Mn(2)-N(21)	2.308(3)	N(24)-Mn(2)-N(23)	89.8(1)	N(25)-Mn(2)-N(21)	75.9(1)
		N(24)-Mn(2)-N(25)	81.5(1)	N(22)-Mn(2)-N(21)	73.6(1)
		N(24)-Mn(2)-N(22)	149.6(1)	S(2)-O(21)-Mn(2)	132.1(2)

Electrospray-ionization mass spectrometry (ESI-MS) Experiments. For ESI-MS experiments, a 2 mM CF_3CH_2OH solution of **2** was prepared under an Ar atmosphere. A 50 µL aliquot of the solution of **2** was diluted into CH_3CN and analyzed by ESI-MS (Figure S2A). (We note that, on the basis of electronic absorption measurements, **2** is less stable in CH_3CN than pure CF_3CH_2OH and begins to decay under these conditions.) A second 50 µL aliquot of **2** was treated with 10 µL of $H_2{}^{18}O$ and then

diluted into CH_3CN. The resulting solution was analyzed by ESI-MS five minutes after the addition of the $H_2{}^{18}O$ (Figure S2B). The remaining solution of **2** decayed to **3** after three hours, and a 20 µL aliquot of the solution of **3** was diluted into CH_3CN for ESI-MS analysis (Figure S2C). Electrospray ionization mass spectrometry experiments were performed using an LCT Primers MicroMass electrospray time-of-flight instrument.

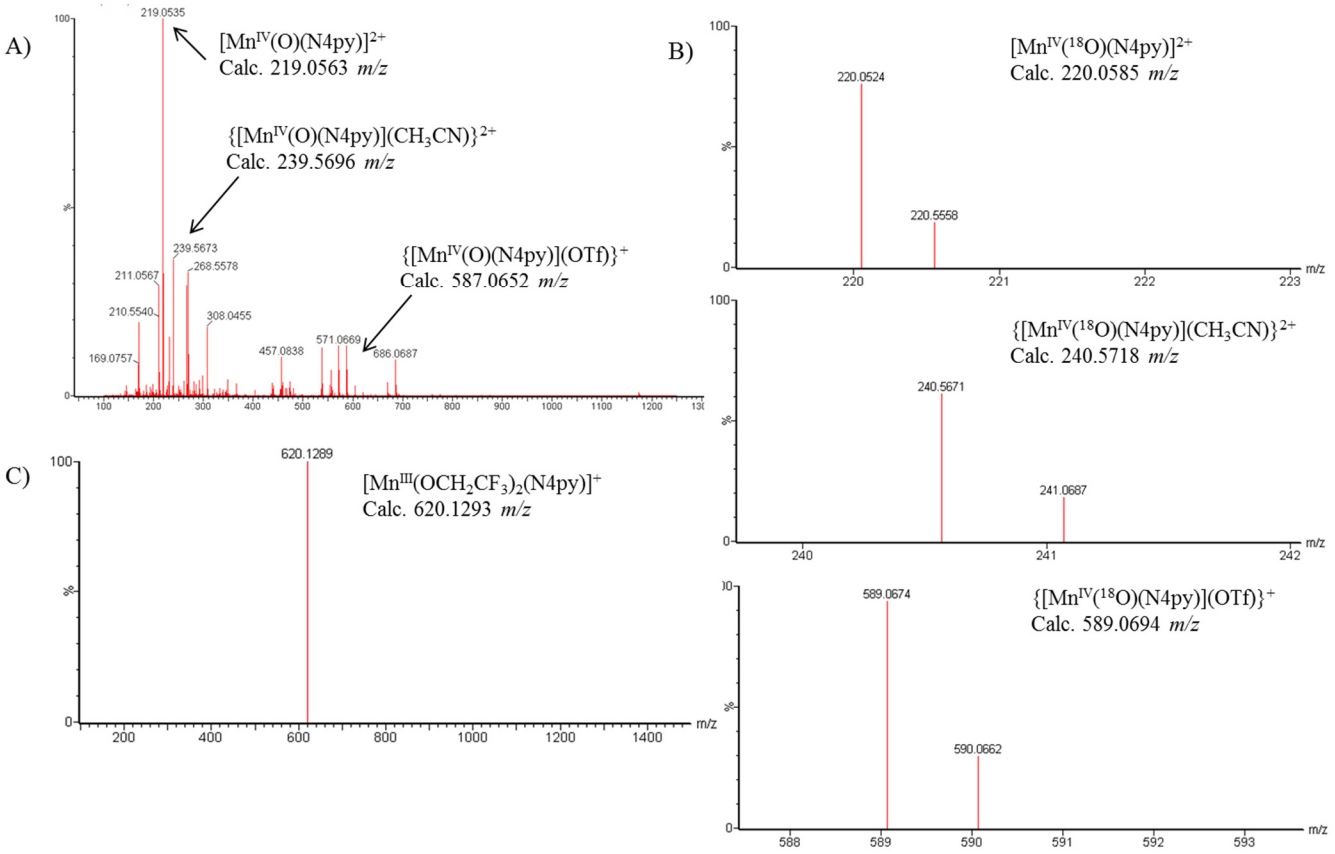

Figure S2. ESI-MS spectra of A) complex **2**, B) its exchange with $H_2{}^{18}O$, and C) complex **3**.

X-band EPR Experiments. 250 µL of a 2 mM CF_3CH_2OH solution of **1** were transferred to a 4 mm quartz EPR tube and flash frozen in liquid N_2. Samples of **2** used for EPR experiments were prepared by adding 2.5 equivalents of PhIO to a 2 mM solution of **1** in CF_3CH_2OH at 25 °C under an Ar atmosphere. After the formation of **2** was judged complete by electronic absorption spectroscopy (~10 min.), 250 µL of the solution were transferred to a 4 mm quartz EPR tube and flash frozen in liquid N_2. The remaining solution of **2** fully decayed to **3** in three hours, as monitored by electronic absorption, and from this solution of **3**, 250 µL were transferred to an EPR tube and flash frozen in liquid N_2.

EPR spectra were collected on an X-band (9 GHz) Bruker EMXPlus spectrometer equipped with an Oxford ESR900 continuous-flow liquid helium cryostat and an Oxford ITC503 temperature system to monitor and regulate the temperature. A dual mode cavity (Bruker ER4116DM) was used for perpendicular and parallel mode detection. Spectra were recorded under non-saturating conditions using 100 kHz field modulation. Other parameters (microwave frequency, modulation amplitude, microwave power, time constant, conversion time, sweep rate, and field resolution) are given in the captions of the corresponding figures. Because the baseline contribution was insignificant, a blank spectrum was not subtracted from the spectra.

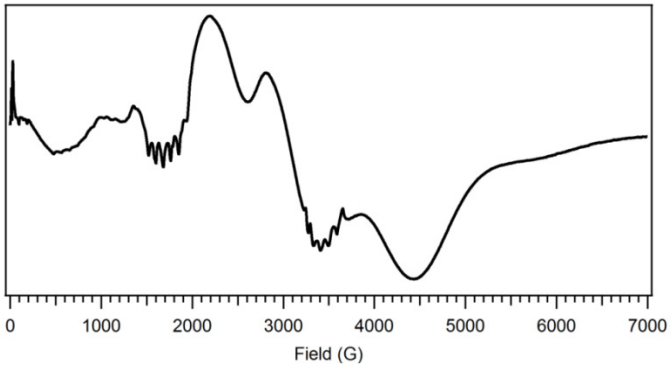

Figure S3. X-band, perpendicular-mode EPR spectrum of a frozen 2 mM CF_3CH_2OH solution of **1**$(OTf)_2$. Recording conditions: T = 5 K, 9.634 GHz microwave frequency, 0.5024 mW microwave power, 6 G modulation amplitude, 100 kHz modulation frequency, 81.92 ms time constant, and 11 667 point resolution.

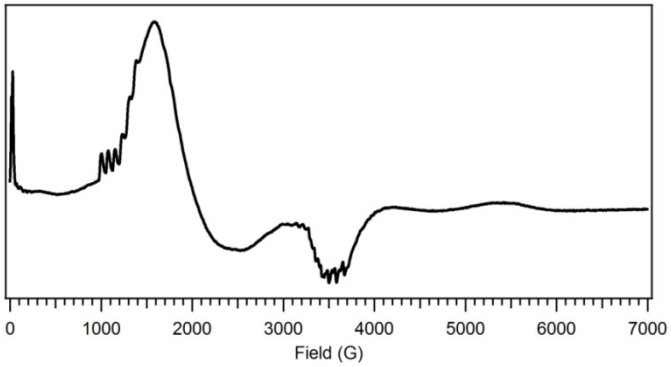

Figure S4. X-band, perpendicular-mode EPR spectrum of a frozen 2 mM CF_3CH_2OH solution of **2**. Recording conditions: T = 5 K, 9.637 GHz microwave frequency, 2.000 mW microwave power, 6 G modulation amplitude, 100 kHz modulation frequency, 81.92 ms time constant, and 11 667 point resolution.

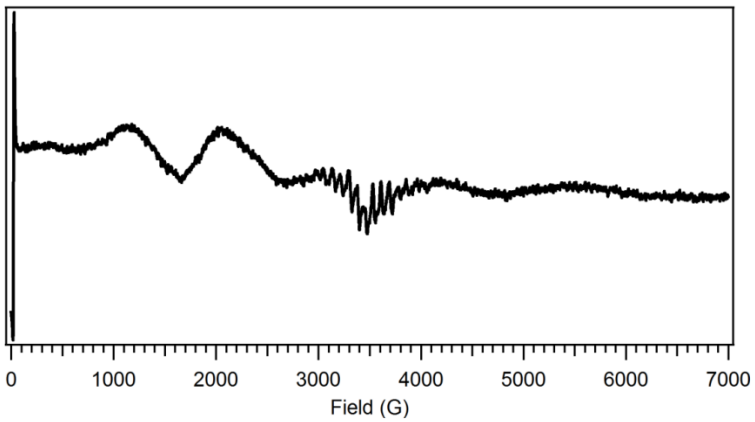

Figure S5. X-band, perpendicular-mode EPR spectrum of a frozen 2 mM CF_3CH_2OH solution of **3**. Recording conditions: T = 5 K, 9.637 GHz microwave frequency, 2.000 mW microwave power, 6 G modulation amplitude, 100 kHz modulation frequency, 81.92 ms time constant, and 11 667 point resolution.

Mn K-edge X-ray absorption (XAS) Experiments. The XAS sample of **1** was prepared by transferring approximately 200 µL of a 10 mM aqueous solution of **1**$(OTf)_2$ to an XAS sample holder which was then flash-frozen in liquid N_2. For the XAS sample of **2**, a 14 mM solution of **1**$(OTf)_2$ in CF_3CH_2OH was treated with 2.5 equivalents of PhIO at 25 ^oC under an Ar atmosphere. Once the formation was complete, three samples were prepared by transferring approximately 400 µL of **2** to each XAS sample holder. All samples were immediately flash-frozen in liquid N_2.

XAS Data Collection. XAS spectra were recorded on beamline X3B at the National Synchrotron Light Source (NSLS), Brookhaven National Lab (storage ring conditions, 2.8 GeV, 100 - 300 mA). Mn K-edge X-ray absorption spectra were recorded on frozen solutions maintained at 20 K with a helium Displex closed-cycle cryostat over the energy range 6.4 – 7.4 keV (Si(111) monochromater). The data were obtained as fluorescence excitation spectra using a solid-state 31-element germanium detector (Canberra). Contamination of higher harmonics radiation was minimized by using a harmonic rejection mirror. Background fluorescence signal was reduced by use of a 6 µm chromium filter for sample **1**. A manganese foil spectrum was recorded concomitantly for internal energy calibration and the first inflection point of the K-edge energy was assigned to 6539.0 eV. Spectra were measured with 5 eV steps below the edge, 0.3 eV steps in the edge region, and steps equivalent to 0.05 $Å^{-1}$ increments above the edge (region borders were 6354, 6529, and 6554 eV). Even under conditions of low X-ray flux, it was observed that complex **2** was slightly photoreduced after each scan as the edge energy shifted ~0.3 eV to lower energy in subsequent scans on the same spot. Thus, the effects of photoreduction on the

XAS data set were minimized by collecting only one scan per sample spot. The XAS spectra of complexes **1** (10 mM in H_2O) and **2** (14 mM in CF_3CH_2OH) represent the average of 7 scans.

EXAFS Data Analysis. Extended X-ray absorption fine-structure (EXAFS) data reduction and averaging were treated entirely using the program EXAFSPAK.[10] Pre-edge background intensity was removed by fitting a Gaussian function to the pre-edge background and subtracting this function from the whole spectrum. The spectrum was then fit with a three-segment spline with fourth-order polynomial components to remove low-frequency background. EXAFS refinement was carried out on $k^3\chi(k)$ data, using phase and amplitude functions obtained from *FEFF*, version 6.[11] The EXAFS fitting was also performed using EXAFSPAK. For each fit, the parameters r (average distance between Mn and scattering atom) and σ^2 (Debye-Waller factor) were optimized, while n, the number of atoms in the shell, was kept fixed. n was varied by integer steps systematically. The goodness-of-fit (GOF) was evaluated by the parameter F, where $F = \Sigma\ (\chi_{calcd} - \chi_{expt})^2 / N$, and N is the number of data points. The threshold energy, E_0, in electronvolts ($k = 0$ point) was kept at a common, variable value for every shell of a given fit.

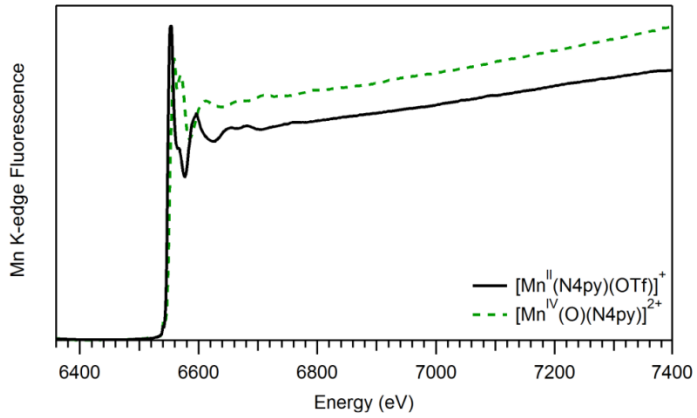

Figure S6. Mn K-edge X-ray absorption spectra of $[Mn^{II}(N4py)(OTf)]^+$ and $[Mn^{IV}(O)(N4py)]^{2+}$.

Table S3. Mn K-edge XAS Near-Edge Properties of $[Mn^{II}(N4py)(OTf)]^+$ and $[Mn^{IV}(O)(N4py)]^{2+}$ and other Mn^{IV}=O complexes.

complex	edge energy (eV)	pre-edge energy (eV)	reference
$[Mn^{II}(N4py)(OTf)]^+$	6547.3	6540.6	[a]
$[Mn^{IV}(O)(N4py)]^{2+}$	6550.8	6541.9	[a]
$[Mn^{IV}(O)(Bn\text{-}TPEN)]^{2+}$	NR[b]	6541.6	12
$[Mn^{IV}(O)(salen)]$	6549.9	6538.9	13
$[Mn^{IV}(O)(T_{piv}PP)]$	6551.2	~6541[c]	14

[a] This work. [b] Not reported. [c] The pre-edge feature for this complex was reported as being "some 10 eV lower in energy than the edge"; see reference 14.

Table S4. EXAFS Fitting Results for $[Mn^{II}(N4py)(OTf)](OTf)$ (**1**$(OTf)_2$) and $[Mn^{IV}(O)(N4py)]^{2+}$ (**2**).[a]

		Mn-O			Mn-N			Mn-C				
complex	fit	*n*	*r*(Å)	σ^2	*n*	*r*(Å)	σ^2	*n*	*r*(Å)	σ^2	E_0	*F*
1$(OTf)_2$	1				6	2.24	9.65				-4.57	113.9
	2	1	2.07	0.96	5	2.25	4.56				-6.24	107.2
	3	1	2.08	1.52	5	2.26	4.99	5	3.11	11.99	-4.93	79.1
	4	1	2.08	1.59	5	2.26	5.03	4	3.11	9.94	-4.97	81.3
	5	1	2.08	1.41	5	2.26	4.92	3	3.11	7.88	-5.14	84.5
	6	***1***	***2.09***	***2.38***	***5***	***2.26***	***5.55***	***3***	***3.00***	***7.06***	***-4.51***	***79.6***
								3	***3.15***	***3.75***		
2	1				6	2.00	11.06				-7.74	445.3
	2	1	1.68	3.91	5	1.98	8.18				-7.36	268.7
	3	1	1.69	4.53	4	2.01	6.18				-1.71	253.1
					1	2.25	3.40					
	4	1	1.68	4.32	4	2.02	6.51	1	2.96	0.75	-0.464	224.6
					1	2.26	2.86					
	5	1	1.68	4.31	4	2.02	6.47	3	2.95	4.79	-0.278	200.2
					1	2.26	2.74					
	6	1	1.68	3.72	5	2.00	8.70	3	2.91	6.14	-4.04	230.2
	7	1	1.68	3.52	5	1.99	8.72	3	2.87	3.59	-4.10	208.1
								1	3.00	-2.40		
	8	1	1.68	3.47	5	1.99	8.84	3	2.83	2.98	-3.94	205.2
								3	2.97	1.00		
	9	1	1.68	3.47	5	1.99	8.82	4	2.82	5.21	-4.08	209.6
								4	2.97	2.68		
	10	1	1.68	3.52	5	1.99	8.67	4	2.75	13.7	-5.00	216.6
								5	2.93	6.54		
	11	1	1.68	3.45	5	1.99	8.85	3	2.80	3.82	-3.97	210.7
								5	2.96	3.91		
	12	***1***	***1.69***	***4.39***	***4***	***2.00***	***6.02***	***3***	***2.82***	***3.74***	***-1.87***	***193.8***
					1	***2.24***	***5.48***	***5***	***2.97***	***3.89***		

[a] Fourier-transform range as follows: **1**$(OTf)_2$: 2 – 11.5 $Å^{-1}$ (resolution 0.167 Å); **2**: 2 – 14 $Å^{-1}$ (resolution 0.131 Å). σ^2 is in units of 10^3 $Å^2$.

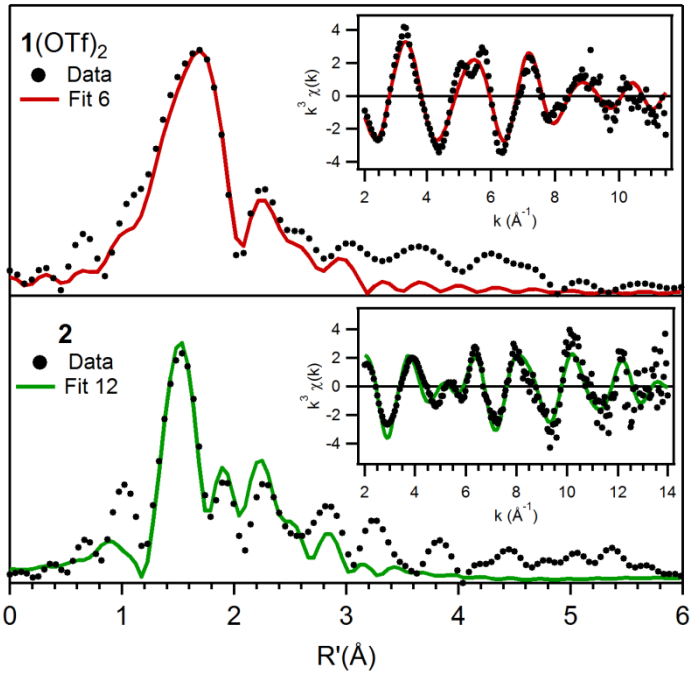

Figure S7. Fourier transforms of Mn K-edge EXAFS data [$k^3\chi(k)$] and raw EXAFS spectra (insets), experimental data (···) and fits (–) for [Mn^{II}(N4py)(OTf)](OTf) (**1**$(OTf)_2$, top) and [Mn^{IV}(O)(N4py)]$^{2+}$ (**2**, bottom). Details regarding EXAFS fits are given in Table S4.

Density Functional Theory Computations for 2. DFT calculations employed the ORCA program package (version 2.8.0).[15] Initial coordinates for **2** were derived from the X-ray structure of [**1**(OTf)]$^+$, where the coordinated triflate was replaced with an oxo ligand. The nuclear coordinates of this model were subjected to full DFT energy minimization and converged to the S = 3/2 ground state, using the BP functional[16] in conjunction with triple-ζ quality TZVP basis sets on Mn, O, and N and SVP basis sets on C and H.[17] The resolution of identity approximation[18] was used to accelerate the calculations using the auxiliary basis set SV/J. The Cartesian coordinates for the geometry-optimized model of **2** are provided in Table S5.

Table S5. Cartesian coordinates (Å) for DFT-optimized structure of $[Mn^{IV}(O)(N4py)]^{2+}$ (**2**).

Atom	x	y	z
Mn	0.000000	0.000000	0.000000
O	0.000000	-0.000000	-1.673290
N	2.000097	0.014236	0.251314
N	0.000000	-2.000888	0.251818
N	-0.090775	2.003667	0.324508
N	-2.004826	0.078980	0.323362
N	0.015103	-0.015765	2.138293
C	2.437871	0.102655	1.539094
C	-0.574706	2.290307	1.565952
C	-0.085096	-2.439032	1.539642
C	-2.294583	0.560283	1.565248
C	-2.990615	-0.289393	-0.519952
C	0.272512	2.991871	-0.518755
C	3.804281	0.014658	1.838801
C	-0.301640	4.649229	1.147097
C	0.015404	-3.804453	1.839939
C	1.383001	0.387134	2.593256
C	-0.379142	-1.386204	2.593125
C	0.165528	-2.881761	-0.764585
C	2.882128	-0.142532	-0.765479
C	4.258607	-0.221833	-0.531232
C	-1.051835	1.044413	2.313049
C	0.188481	-4.725198	0.792955
C	-4.651608	0.273273	1.145842
C	4.726257	-0.148949	0.791363
C	-4.337268	-0.203222	-0.136233
C	0.257752	-4.257333	-0.529764
C	0.177792	4.337636	-0.134630
C	-0.690040	3.608967	2.014981
C	-3.613970	0.667284	2.014232
H	-2.669446	-0.640739	-1.511425
H	0.626274	2.671780	-1.509658
H	4.144353	0.080240	2.883039
H	-0.381249	5.697254	1.473147
H	-0.047580	-4.144639	2.884298
H	1.642302	-0.102081	3.554741
H	1.379460	1.479466	2.792062
H	0.110421	-1.641836	3.555411
H	-1.471814	-1.390081	2.789995
H	0.221539	-2.434459	-1.768285
H	2.435035	-0.202154	-1.769058
H	4.948910	-0.345629	-1.377864
H	-1.278813	1.269703	3.376158
H	0.268642	-5.800942	1.010718
H	-5.700223	0.346143	1.471721
H	5.802807	-0.218849	1.008701
H	-5.124154	-0.502924	-0.843235
H	0.388752	-4.946765	-1.376023
H	0.473203	5.127043	-0.840859
H	-1.078797	3.826178	3.020792
H	-3.833666	1.053766	3.020358

Table S6. Manganese-Ligand Bond Lengths (Å) for $[Mn^{II}(N4py)(OTf)](OTf)$ (**1**$(OTf)_2$) and $[Mn^{IV}(O)(N4py)]^{2+}$ (**2**) Obtained from X-ray Diffraction (XRD), Mn K-edge XAS Data (EXAFS) and DFT Geometry Optimization.

	1$(OTf)_2$ (XRD)	**1**$(OTf)_2$ (EXAFS)	**2** (EXAFS)	**2** (DFT)
Mn–O[a]	2.107	2.09	1.69	1.673
Mn–N_{ax}	2.258	2.26	2.24	2.138
Mn–N_{eq}[b]	2.308	2.26	2.00	2.024

[a] The O atom derives from a triflate and terminal oxo ligand for **1** and **2**, respectively. [b] The average distance of all equatorial Mn–N bond lengths is listed.

3. Kinetic Measurements.

DHA and d_4-DHA. All kinetic measurements were performed under an Ar atmoshphere. 2.9 mg of **1**$(OTf)_2$ and 2.2 mg (2.5 equivalents) of PhIO were each dissolved in 1 mL deoxygenated CF_3CH_2OH. These solutions were combined, stirred for five minutes, and transferred to a UV-Vis cuvette at 25 °C. The formation of **2** ([**2**] = 2 mM) was monitored by the growth of the broad absorption band at 950 nm. Once the formation of **2** was complete, 100 µL of dichloromethane (CH_2Cl_2) containing the substrate (DHA or d_4-DHA) was added and the reaction was monitored by following the decay of the band at 950 nm. Under these conditions, and using varying concentrations of substrate ([DHA] = 0.020 – 0.050 M and [d_4-DHA] = 0.020 - 0.040 M) complex **2** showed pseudo-first order decay to at least four half-lives. The second-order reaction rate k_2 was calculated from a linear correlation between the substrate concentration and the observed rate and corrected for the number of reactive C-H bonds to yield k_2' (Table S7). From the k_2 values obtained from these linear plots for DHA (k_2 = 3.6 M^{-1} s^{-1}) and d_4-DHA (k_2 = 0.32 M^{-1} s^{-1}), the kinetic isotope effect (KIE) was calculated to be 11.2.

The effect of solvent on the rate of substrate oxidation by **2** was investigated by forming **2** in a CF_3CH_2OH:CH_2Cl_2 1:1 (volume:volume) solvent mixture under the same conditions as above. Once the formation of **2** was completed, 100 µL of dichloromethane (CH_2Cl_2) containing DHA ([DHA] = 0.020 – 0.050 M) or d_4-DHA ([d_4-DHA] = 0.020 – 0.040 M) were added and the reaction was monitored by following the decay of the band at 950 nm. The second-order reaction rates for DHA (k_2 = 2.61 M^{-1} s^{-1}) and d_4-DHA (k_2 = 0.30 M^{-1} s^{-1}) were calculated from the linear correlation between the substrate concentration and the observed rate (Figure S9). The KIE was determined to be 8.7 (Table S7). Formation of **2** in a CF_3CH_2OH:$(CH_3)_2NC(O)H$ (1:1 volume:volume) solvent mixture was unsuccessful. Although it was possible to form **2** in CF_3CH_2OH:CH_3CN (1:1 volume:volume) and CF_3CH_2OH:$(CH_3)_2CO$ (1:1 volume:volume) solvent mixtures, the stability of **2** was greatly reduced, hampering any kinetic experiments.

The activation parameters of hydrogen-atom abstraction for the reactions of **2** (1 mM) with DHA (0.01 M) and d_4-DHA (0.01 M) were determined from experiments in a CF_3CH_2OH:CH_2Cl_2 (1:1) solvent mixture in the temperature range of 268 – 308 K. The decay of **2** was monitored by electronic absorption and the pseudo-first order rate constant was calculated for each reaction at each temperature (Figure S10 and Table S9-10).

Other organic substrates. The reactions of **2** in a deoxygenated CF_3CH_2OH:CH_3CN 19:1 (volume:volume) mixture with 0.150 mL of CF_3CH_2OH:CH_3CN (19:1) containing the substrate (ethylbenzene, diphenylmethane, and toluene) were also monitored by electronic absorption spectroscopy. Under the conditions of these reactions ([ethylbenzene] = 0.10 – 0.40 M, [diphenylmethane] = 0.10 – 0.22 M, and ([toluene] = 0.40 – 0.70 M), **2** decayed with pseudo-first order behavior to at least four half-lives, and a linear relationship was observed between the substrate concentration and the pseudo-first-order rate constant (Figure S8). The second-order rate constants determined from this relationship were corrected for the number of reactive C-H bonds (Table S7).

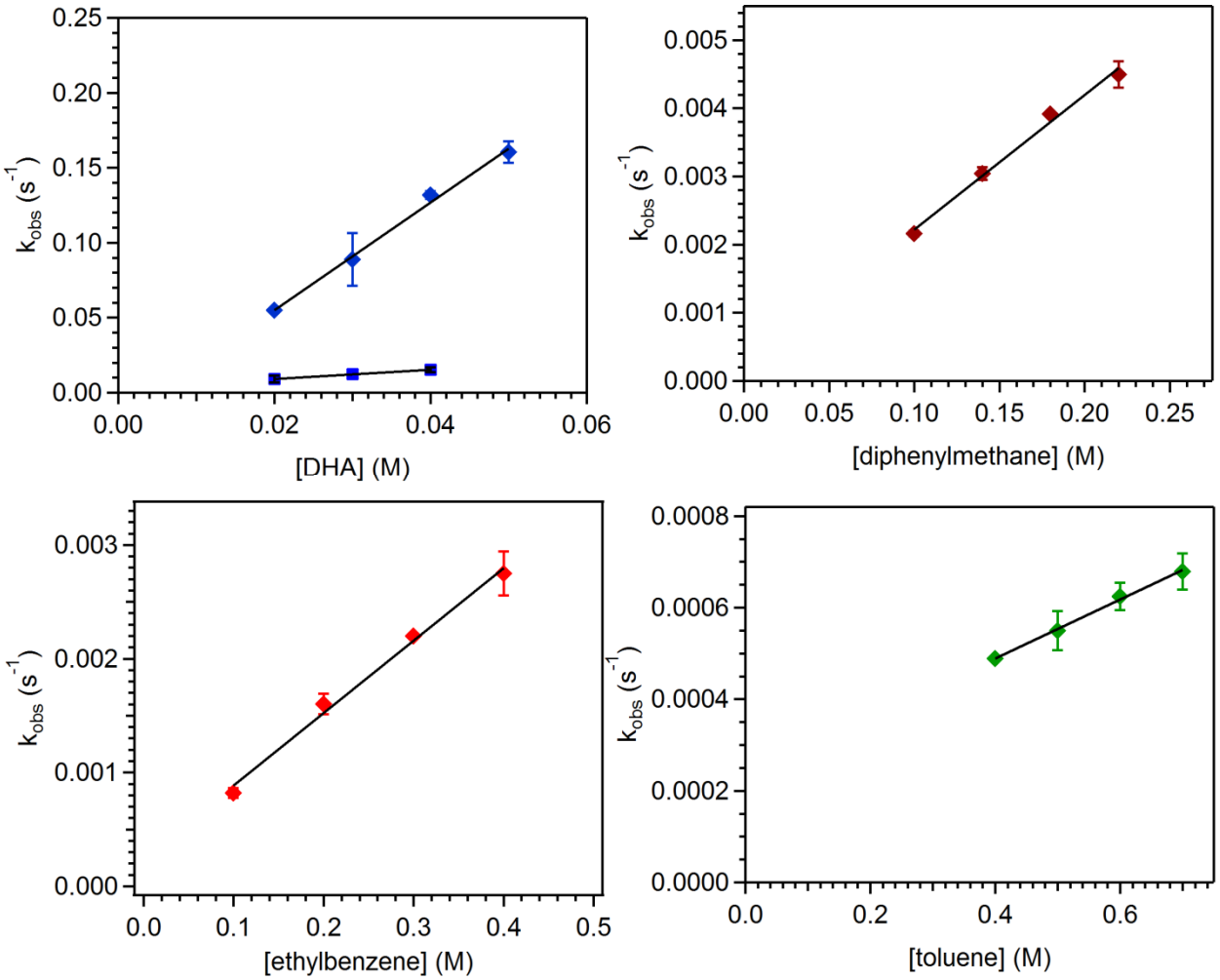

Figure S8. Plots of pseudo-first order rate constants, k_{obs} (s^{-1}), against substrate concentration for a 1.9 mM solution of **2** in CF_3CH_2OH:CH_2Cl_2 (19:1) for (a) DHA and d_4-DHA and for a 2 mM solution of **2** in CF_3CH_2OH:CH_3CN (19:1) for (b) diphenylmethane, (c) ethylbenzene, and (d) toluene. The second-order rate constant, k_2 (M^{-1} s^{-1}), was calculated from the linear correlation of the observed rate and substrate concentration.

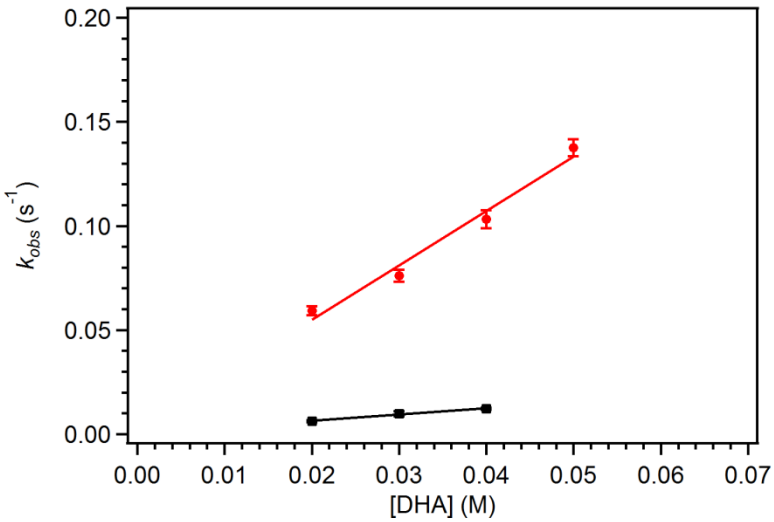

Figure S9. Pseudo-first order rate constants, k_{obs} (s^{-1}) versus substrate concentration for a 1.9 mM solution of **2** in CF_3CH_2OH:CH_2Cl_2 (1:1) for DHA (red dots) and d_4-DHA (black squares). The second-order rate constant, k_2 (M^{-1} s^{-1}), was calculated from the linear correlation of the observed rate and substrate concentration.

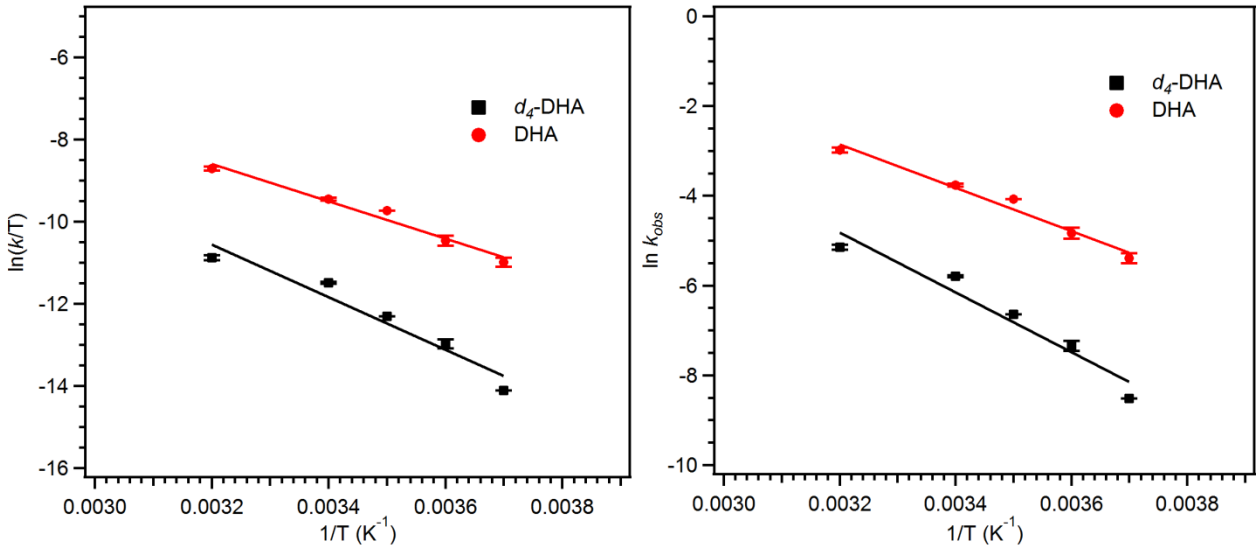

Figure S10. Eyring plots (left) and Arrhenius plots (right) for the hydrogen atom abstraction of DHA (0.01 M, red dots) and d_4-DHA (0.01 M, black squares) by complex **2** (1 mM) in CF_3CH_2OH:CH_2Cl_2 (1:1).

Table S7. Corrected Second-order Rate Constants (k_2')[a] for Reaction of **2** with DHA, d_4-DHA, ethylbenzene, diphenylmethane, and toluene.

Substrate	k_2 ($M^{-1}s^{-1}$)	k_2' ($M^{-1}s^{-1}$)
DHA	3.6	0.90
d_4-DHA	0.32	0.079
diphenylmethane	0.020	0.0099
ethylbenzene	0.0057	0.0019
toluene	0.00064	0.00021

[a] (k_2') is the second-order rate constant corrected for the number of reactive C-H bonds.

Table S8. Corrected Second-order Rate Constants (k_2) for Reaction of Mn^{IV}=O Complexes with DHA at the Temperature Indicated.

complex[a] [concentration]	k_2' ($M^{-1}s^{-1}$)	T (*K*)	solvent	KIE	ref
$[Mn^{IV}(O)(OH)(TF_4TMAP)]^{3+}$ [0.01 mM]	1.22	288	H_2O:MeCN (2:1)	8	19
$[Mn^{IV}(O)(N4py)]^{2+}$ [1.9 mM]	0.90	298	CF_3CH_2OH: CH_2Cl_2 (20:1)	11.2	[b]
$[Mn^{IV}(O)(N4py)]^{2+}$ [1.9 mM]	0.65	298	CF_3CH_2OH: CH_2Cl_2 (1:1)	8.7	[b]
$[Mn^{IV}(O)(OH_2)(BQCN)]^{2+}$ [2 mM]	0.030	273	MeCN:H_2O (9:1)		20
$[Mn^{IV}(O)(H_3buea)]^{-}$ [0.6 mM]	0.026	293	DMSO	6.8	21
$[Mn^{IV}(O)_2(Me_2EBC)]$ [2 mM]	0.01496	288	$(CH_3)_2CO$:H_2O (4:1)	3.78	22
$[Mn^{IV}(O)(OH)(^{H,Me}Pytacn)]^{+}$ [1 mM]	0.0065	298	MeCN:H_2O (4:1)	3.1	23

[a] Ligand abbreviations: TF_4TMAP = meso-tetrakis(2,3,5,6-tetrafluoro-*N,N,N*-trimethyl-4-aniliniumyl)porphyrinato dianion; N4py = *N*,*N*-bis(2-pyridylmethyl)-*N*-bis(2-pyridyl)methylamine; BQCN = *N*,*N*′-dimethyl- *N*,*N*′-bis(8-quinolyl)cyclohexanedimaine; H_3buea = tris[(*N*′-*tert*-butylureaylato)-*N*-ethylene]aminato; Me_2EBC = 4,11-dimethyl-1,4,8,11-tetraazabicyclo[6.6.2]hexadecane; ^{H,Me}Pytacn = 1-(2-pyridylmethyl)-4,7-dimethyl-1,4,7-triazacyclononane. [b] This work.

Table S9. Kinetic Parameters for Reaction of Mn^{IV}=O Complexes with DHA.

complex[a] [concentration]	solvent	$\Delta G^{\ddagger}$ [b]	$\Delta H^{\ddagger}$ [b]	$\Delta S^{\ddagger}$ [c]	ref
$[Mn^{IV}(O)(N4py)]^{2+}$ [1.0 mM]	CF_3CH_2OH:CH_2Cl_2 (1:1)	19.4 ± 0.8	9 ± 0.8	-35 ± 3	[d]
$[Mn^{IV}(O)(H_3buea)]^{-}$ [0.6 mM]	DMSO	19.6 ± 1	5 ± 1	-49 ± 4	21
$[Mn^{IV}(O)_2(Me_2EBC)]$ [2 mM]	$(CH_3)_2CO$:H_2O (4:1)	21.0 ± 0.6	13.7 ± 0.6	-24.5 ± 2.2	24
$[Mn^{IV}(O)(OH)(^{H,Me}Pytacn)]^{+}$ [1 mM]	MeCN:H_2O (4:1)	21.3 ± 0.7	10.3 ± 0.7	-37 ± 2	23

[a] Ligand abbreviations are the same as those given for Table S8. [b] kcal/mol (at 25 °C for $\Delta G^{\ddagger}$). [c] cal / mol K [d] This work.

Table S10. Activation Parameters for Reaction of Mn^{IV}=O Complexes with DHA and d_4-DHA.

complex[a] [concentration]	E_H [b]	E_D [b]	A_H [c]	A_D [c]	A_H/A_D	ref
$[Mn^{IV}(O)(N4py)]^{2+}$ [1.0 mM][d]	9.6 ± 0.9	13.2 ± 1.9	2.9 x 10^5	1.4 x 10^7	0.021	[f]
$[Mn^{IV}(O)_2(Me_2EBC)]$ [2 mM][e]	14.3 ± 0.6	20.3 ± 0.5	7.6 x 10^7	7.3 x 10^{11}	1.1 x 10^{-4}	24

[a] Ligand abbreviations are the same as those given for Table S8. [b] kcal/mol. [c] s^{-1}. [d] solvent: CF_3CH_2OH:CH_2Cl_2 (1:1). [e] solvent: $(CH_3)_2CO$:H_2O (4:1). [f] This work.

Product analysis and final oxidation state of manganese. 2.9 mg of **1**$(OTf)_2$ and 2.2 mg of PhIO were each dissolved in 1 mL deoxygenated CF_3CH_2OH under an Ar atmosphere and were combined, stirred for ten minutes ([**2**] = 2 mM), and treated with 7.5 mg DHA (10 equivalents) in 100 µL of deoxygenated CH_2Cl_2. After 30 min, the solvent was removed and the organic products were redissolved in 2 mL of cyclohexane. The anthracene produced by the reaction of **2** with DHA was quantified by measuring the absorbance of the cyclohexane solution of the organic products at 356 nm, yielding 1.1 ± 0.15 mM anthracene (average of 6 different experiments).

The final oxidation state of the manganese was determined using an iodometric titration.[25] 2.9 mg of **1**$(OTf)_2$ and 2.2 mg of PhIO were each dissolved in 1 mL deoxygenated CF_3CH_2OH under an Ar atmosphere and were combined, stirred for ten minutes ([**2**] = 2 mM), and treated with 7.5 mg DHA (10 equivalents) in 100 µL of deoxygenated CH_2Cl_2. After 30 min, the solvent was removed and the organic products were removed from the manganese product (**3**) by rinsing the residue with diethyl ether (3 × 5 mL). The residue was dried and redissolved in 2 mL of CH_2Cl_2 and a 1 mL aliquot was transferred to a 10 mL volumetric flask containing 1 mL glacial acetic acid and 0.019 g tetrabutylammonium iodide, followed by dilution with CH_2Cl_2 up to 10 mL. The bright yellow solution was mixed and the absorbance was measured in a 0.5 cm cuvette at 25 °C immediately after mixing. The triiodide produced was quantified by measuring the absorbance of the solution at 295 and 365 nm and the final oxidation state of the manganese was determined by the ratio of the triiodide liberated and the Mn^{IV} consumed.[25] The final oxidation state of **3** was 2.7 ± 0.15 (average of 5 different experiments).

Cyclic voltammetry. The electrochemical properties of complex **2** were investigated by cyclic voltammetry. Complex **2** exhibits a one-electron redox process at 0.370 V versus Cp_2Fe/Cp_2Fe^+ (0.8 V versus SCE) in CF_3CH_2OH:CH_2Cl_2 (1:1 with 0.1 M NBu_4PF_6), which was assigned to the $Mn^{III}(O)/Mn^{IV}(O)$ couple (Figure S11). The redox wave is partially reversible at 50 and 100 mV s^{-1} scan velocities. An irreversible reduction process is also observed at E_{pc} = -0.260 V versus Cp_2Fe/Cp_2Fe^+, which is

attributed to the reduction of excess iodosylbenzene (Figure S11). Complex **2** exhibits a higher reduction potential than $[Mn^{IV}(O)(H_3buea)]^-$ ($E_{1/2}$ = -1.0 V versus Cp_2Fe/Cp_2Fe^+; -0.570 V versus SCE)[21] and $[Mn^{IV}(O)(OH)(^{H,Me}Pytacn)]^+$ ($E_{1/2}$ = -0.38 V versus Cp_2Fe/Cp_2Fe^+; 0.05 V versus SCE).[23]

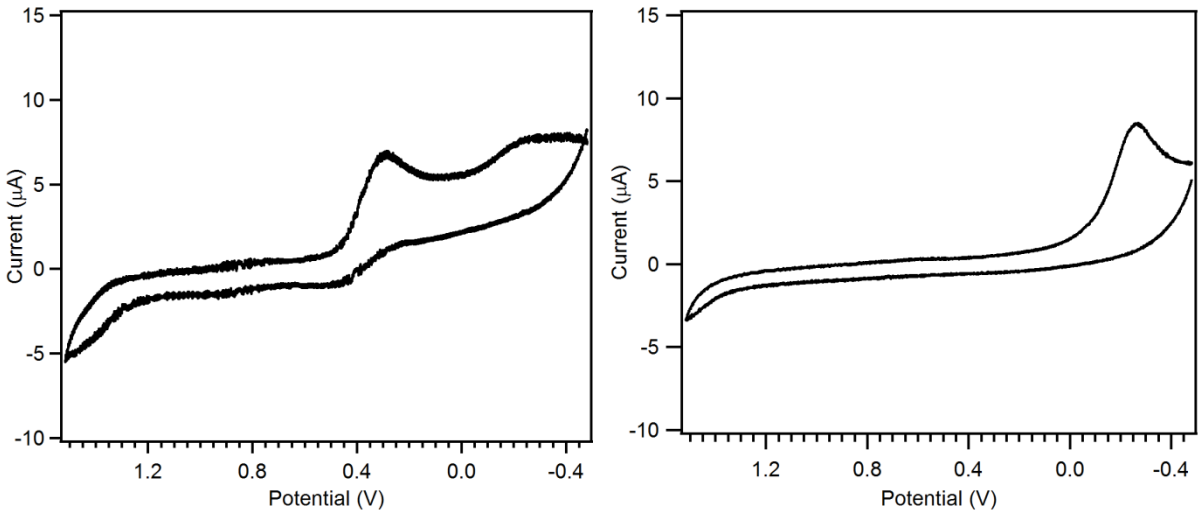

Figure S11. Cyclic voltammograms of **2** (left) and PhIO (right) recorded in CF_3CH_2OH:CH_2Cl_2 (1:1 with 0.1 M NBu_4PF_6) at 50 mV s^{-1}. The cyclic voltammogram of PhIO was collected under the same conditions as for complex **2**, without the addition of **1**.

4. References

1. D. D. Perrin and W. L. F. Armarego, *Purification of Laboratory Chemicals*, Butterworth-Heinemann, Oxford, U.K., 1997.

2. C. R. Goldsmith, R. T. Jonas and T. D. P. Stack, *Journal of the American Chemical Society*, 2001, **124**, 83-96.

3. J. Chang, S. Plummer, E. S. F. Berman, D. Striplin and D. Blauch, *Inorg. Chem.*, 2004, **43**, 1735-1742.

4. M. Lubben, A. Meetsma, E. C. Wilkinson, B. Feringa and L. Que, *Angew. Chem.-Int. Edit. Engl.*, 1995, **34**, 1512-1514.

5. R. A. Geiger, D. F. Leto, S. Chattopadhyay, P. Dorlet, E. Anxolabéhère-Mallart and T. A. Jackson, *Inorg. Chem.*, 2011, **50**, 10190-10203.

6. International Tables for Crystallography, Vol A, 4th ed., Kluwer: Boston (1996).

7. Data Collection: SMART Software Reference Manual (1998). Bruker-AXS, 5465 E. Cheryl Parkway, Madison, WI 53711-5373 USA.

8. Data Reduction: SAINT Software Reference Manual (1998). Bruker-AXS, 6300 Enterprise Dr., Madison, WI 53719-1173, USA.

9. G. M. Sheldrick (2000). SHELXTL Version 6.10 Reference Manual. Bruker-AXS, 5465 E. Cheryl Parkway, Madison, WI 53711-5373 USA.

10. G. N. George, in *EXAFSPAK*, Stanford Synchrotron Radiation Laboratory; Stanford, CA, 1990.

11. J. J. Rehr, J. Mustre de Leon, S. I. Zabinsky and R. C. Albers, *J. Am. Chem. Soc.*, 1991, **113**, 5135-5140.

12. X. Wu, M. S. Seo, K. M. Davis, Y.-M. Lee, J. Chen, K.-B. Cho, Y. N. Pushkar and W. Nam, *J. Am. Chem. Soc.*, 2011, **133**, 20088-20091.

13. T. Kurahashi, A. Kikuchi, T. Tosha, Y. Shiro, T. Kitagawa and H. Fujii, *Inorg. Chem.*, 2008, **47**, 1674-1686.

14. K. Ayougou, E. Bill, J. M. Charnock, C. D. Garner, D. Mandon, A. X. Trautwein, R. Weiss and H. Winkler, *Angew. Chem. Int. Ed.*, 1995, **34**, 343-346.

15. F. Neese, *ORCA - an ab initio, Density Functional and Semiempirical Program Package*, *Version 2.9*, Max Planck Institute for Bioinorganic Chemistry, 2012.

16. a) A. D. Becke, *J. Chem. Phys.*, 1986, **84**, 4524-4529; b) J. P. Perdew, *Physical Review B*, 1986, **33**, 8822-8824.

17. a) A. Schäfer, H. Horn and R. Ahlrichs, *J. Chem. Phys.*, 1992, **97**, 2571-2577; b) A. Schäfer, C. Huber and R. Ahlrichs, *J. Chem. Phys.*, 1994, **100**, 5829-5835.

18. F. Neese, *J. Comput. Chem.*, 2003, **24**, 1740-1747.

19. C. Arunkumar, Y.-M. Lee, J. Y. Lee, S. Fukuzumi and W. Nam, *Chem. Eur. J.*, 2009, **15**, 11482-11489.

20. S. C. Sawant, X. Wu, J. Cho, K.-B. Cho, S. H. Kim, M. S. Seo, Y.-M. Lee, M. Kubo, T. Ogura, S. Shaik and W. Nam, *Angew. Chem. Int. Ed.*, 2010, **49**, 8190-8194.

21. T. H. Parsell, M.-Y. Yang and A. S. Borovik, *J. Am. Chem. Soc.*, 2009, **131**, 2762-2763.

22. G. Yin, A. M. Danby, D. Kitko, J. D. Carter, W. M. Scheper and D. H. Busch, *J. Am. Chem. Soc.*, 2008, **130**, 16245-16253.

23. I. Garcia-Bosch, A. Company, C. W. Cady, S. Styring, W. R. Browne, X. Ribas and M. Costas, *Angew. Chem. Int. Ed.*, 2011, **50**, 5648-5653.

24. Y. Wang, S. Shi, H. Wang, D. Zhu and G. Yin, *Chem. Commun.*, 2012, **48**, 7832-7834.

25. J. F. Perez-Benito, E. Brillas and C. Arias, *Canadian Journal of Chemistry*, 1990, **68**, 79-81.